

**Sound Velocity of Aragonite (CaCO<sub>3</sub>) at High Pressure and High  
Temperature and Implications for Low Velocity Zone in the Subduction  
Zone**

**Ying Li<sup>1,2</sup>, Fengxia Sun<sup>1,3</sup>, Yongtao Zou<sup>5</sup>, Ting Chen<sup>2</sup>, Xintong Qi<sup>2</sup>, Haiyan  
Chen<sup>2</sup>, Songlin Xu<sup>2</sup>, Nao Cai<sup>2</sup>, Jianguo Du<sup>1,3</sup>, Baosheng Li<sup>2,4</sup>**

<sup>1</sup> United Laboratory of High-Pressure Physics and Earthquake Science, Key  
Laboratory of Earthquake Prediction, Institute of Earthquake Forecasting, CEA,  
Beijing, China

<sup>2</sup> Mineral Physics Institute, State University of New York, Stony Brook, New York  
11794, USA

<sup>3</sup> School of Earth Sciences and Resources, China University of Geoscience (Beijing),  
Beijing, China

<sup>4</sup> Department of Geosciences, State University of New York, Stony Brook, New  
York, USA

<sup>5</sup> Shenzhen Key Laboratory of Ultraintense Laser and Advanced Material  
Technology, and College of Engineering Physics, Shenzhen Technology University,  
Shenzhen 518118, China

Corresponding author: Ying Li ([subduction6@hotmail.com](mailto:subduction6@hotmail.com)) & Fengxia Sun  
([396425908@qq.com](mailto:396425908@qq.com))

**Key Points:**

- Velocities of aragonite and subsequent elastic moduli are obtained at high pressure and high temperature.
- Aragonite has low V<sub>p</sub>, V<sub>s</sub> and high V<sub>p</sub>/V<sub>s</sub> compared with other minerals in subduction zone.
- 2.5wt.% of aragonite in carbonated-ocean crust would enhance the observations of Low velocity layer in subduction zone significantly.

## Abstract

By using the combined ultrasonic interferometry and X-ray diffraction method, the elastic wave velocities of aragonite were measured for the first time at pressure and temperature up to 5.8 GPa and 1173 K by using a hot-pressed polycrystalline specimen. Aragonite has extremely low compressional ( $V_p$ ) and shear ( $V_s$ ) wave velocities and  $V_p$ , low  $V_s$  and high  $V_p/V_s$  ratio than those of the major minerals of subduction slabs. According to the average content of  $\text{CO}_2$  in the subduction zones, the velocities of carbonated-eclogite and carbonated-peridotite in both cold and hot subduction zones were modeled. It was revealed that an increase of 2.5 wt%  $\text{CO}_2$  resulted in to 2% reduction in  $V_p$  and  $V_s$  and an increase of  $V_p/V_s$ . Our results show that the velocity effect of aragonite in subduction zone can't be ignored and shed lights on the mechanism of low velocity layers (LVL) in the subduction zones.

## Plain Language Summary

Low velocity layers extend beyond 150 km are widely distribute along subducted slabs around pacific ocean, the origin of which was attributed to hydrous minerals. Aragonite is ubiquitous in the marine sediment and carbonated oceanic crust, however, the velocities and the effect on subduction zone are rarely discussed . Here we measured the velocities of aragonite at high pressure and temperature conditions. The measured velocities of compressional ( $V_p$ ) and shear ( $V_s$ ) wave of the aragonite are respectively 26 ~ 33% and 23 ~33% lower than those of the major minerals of subduction slabs. Furthermore, aragonite exhibits a large  $V_p/V_s$  that 5% ~ 9% higher than those for major subduction slab minerals. The experiment results were applied to the calculation of carbonated oceanic crust and carbonated mantle, found that the practical content of aragonite in subduction zone would cause 2% in  $V_p$  and  $V_s$  reduction and a increase in  $V_p/V_s$  ratio. Our findings suggest that velocity effect of small amount of aragonite in subduction zone is unnegligible.

## 1 Introduction

Carbon is an essential and primary element to many geological processes. The storage, dissolution and release of carbon in the deep earth has been proposed to be the critical mechanisms of the global carbon cycle (Molina and poli, 2000; Frezzotti et al., 2011, Kelemen and Manning, 2015). The dominative source of carbon in the atmosphere is outgassing from the Earth's interior at midocean ridges, hotspot volcanoes, subduction-related volcanic arcs, and even the seismic active faults in the non-volcanic area (Li et al., 2013). Much of the  $\text{CO}_2$  released at subduction zones is derived from the metamorphism of carbonate rocks subducted with the ocean crust.  $\text{CaCO}_3$ , one of the most abundant carbonates near the Earth's surface, has been identified to be a dominant carbon-bearing mineral in the crust, mainly in carbonated-

basaltic oceanic crust and carbon-bearing sediments (Kelemen and Manning, 2015). The polymorphic phases of  $\text{CaCO}_3$  (e.g., calcite, aragonite and vaterite) can be transported to deeper depths and become decarbonized in the subduction zone (Perchuk and Korepanova, 2011). The recent joint experimental and first-principal study indicated that  $\text{CaCO}_3$  could be stable up to  $P \sim 105$  GPa and  $T \sim 2000$  K, corresponding to the pressure close to the core-mantle boundary (Lobanov et al., 2017).

Aragonite remains stable in a wide P-T conditions corresponding to the lower crust and the uppermost mantle. It can be kept metastable up to 38 GPa at room temperature and then transforms into post-aragonite structure (Ono et al., 2005). Aragonite sedimentation in the pelagic realm is about 12% at least relative to calcite on a worldwide, such as in the sediment samples collected from Atlantic and the Pacific sediment traps, as well as the plankton and some rare pelagic sediments (Berner and Honjo, 1981). In addition, the sediments and altered oceanic crusts have mostly been subjected to a relatively high P-T condition (400 ~ 500°C and ~1.0 GPa), which is sufficient for the phase transformation of calcite to aragonite to occur. The investigations of metamorphic devolatilization of subducted lithologies on all the representative marine sediments, including the global average marine sediment, clay carbonate from Antilles, siliceous limestone from Marianas, and carbonate ooze from Vanuatu, indicate that aragonite is the unique carbon bearing phase after the metamorphism of subducted sediments in subduction zones up to the P-T conditions of 6 GPa and 900°C, and accounts for the  $2.5 \sim 3.5 \times 10^{12}$  mol  $\text{yr}^{-1}$  carbon budget imbalance in subduction zone (Kerrick and Connolly, 2001). The samples from Ocean Drilling Program/Integrated Ocean Drilling Program (ODP/IODP) show direct evidence of  $\text{CO}_2$  presence in the ocean crust, which contains approximately 2% ~ 3% carbonates in the uppermost volcanic section and brings approximately  $2.9 \pm 0.4 \times 10^{12}$  mol C/y into the subduction zone (Alt and Teagle, 1999; Shilobreeva et al., 2011). Thus, aragonite has a profound effect on fluid generation, arc magma evolution, global carbon cycle, and physical and chemical properties of the subduction zones.

Elastic properties of minerals are the keys to understanding the Earth's composition and dynamics by comparing with the velocity profiles of the Earth's interior attained by seismological surveys (Li et al., 2005). The elastic properties of aragonite have been studied by the various methods, such as Brillouin spectroscopy (Liu et al., 2005), static compression X-ray diffraction (Martinez et al., 1996; Santillán and Williams, 2004; Ono et al., 2005; Li et al., 2015; Litasov et al., 2017) and theoretical calculations and models (Fisler et al., 2000; Santos et al., 2020), providing valuable data on the bulk modulus, unit-cell volume and thermal expansion at high pressure. However, the very limited information on the shear elastic properties, especially at simultaneous high pressure and temperature was reported.

Elasticity and velocities of carbonates have significant influence on the properties of subduction zones (Sanchez-Valle et al., 2011; Yang et al., 2014; Zhao et al., 2019). Worthy of particular mention is that the velocities of calcite are lower than those of most major mantle minerals, and the phase transition of calcite I to calcite II at high pressures may cause sharp decrease or discontinuity in seismic wave velocities (Kondo et al., 1972). Chen et al. (2006) reported the elasticity of dolomite at ambient pressure and temperature using Brillouin spectroscopy is between those of calcite and magnesite ( $\text{MgCO}_3$ ). By comparison, the elastic moduli of magnesite are close to those of the major minerals in peridotite and eclogite so that the velocity difference between 10 wt.% magnesite-bearing eclogite (peridotite) and pure eclogite (peridotite) is less than 1% (Litasov et al., 2008; Yang et al., 2014). Additionally, Brillouin scattering spectroscopy investigation on the velocities of ferromagnesian carbonates with different iron contents indicated that the substitutions of Fe for Mg may reduce the velocity of magnesite (e.g., Sanchez-Valle et al., 2011).

In this study, ultrasonic interferometric measurements on aragonite were conducted using a high-quality hot-pressed polycrystalline specimen up to 5.8 GPa and 1173 K. For the first time, the densities, elastic bulk and shear moduli and their pressure and temperature derivatives of the aragonite sample were simultaneously determined. By using our experimental data and combining with other major constituent minerals of subduction zone, the P and S velocities of carbonated-eclogite and carbonated-peridotite along subduction geotherm were modeled. Our results allowed us to evaluate the effect of aragonite on seismic structures in subduction zones.

## 2 Experiment methods

The experimental set-up and pressure - temperature (P-T) conditions have been described in detail (Li et al., 2015). The polycrystalline specimen of aragonite was hot pressed under pressure of 8 GPa and temperature of  $\sim 700$  K using reagent-grade calcite powder and the 1000-ton uniaxial split-cylinder apparatus (USCA-1000) in the High Pressure Laboratory of Stony Brook University. The bulk density attained by Archimedes immersion ( $2.92(1) \text{ g/cm}^3$ ) agrees well ( $\sim 0.5\%$ ) with the value derived from X-ray diffraction measurement ( $2.932 \text{ g/cm}^3$ ) from this study, and within 0.2-0.4% of the theoretical density ( $2.926 \sim 2.933 \text{ g/cm}^3$ ) attained by Huggins (1922). The sample was shaped into a cylindrical disk with both surfaces polished, the final thickness after polishing is  $0.957(1) \text{ mm}$ .

The high-pressure and high-temperature in situ experiments were conducted at the X17B2 beamline of the Brookhaven National Laboratory (BNL) using a DIA-type cubic-anvil apparatus. Details of the experimental set-up can be found elsewhere (Weidner et al. 1992; Li et al. 2004; Li et al., 2015). The pressure-transmitting medium

was made of boron and epoxy mixture (4:1 wt.% ratio) pre-compressed into cubic shape with an edge length about 6.4 mm. The aragonite specimen was embedded in a NaCl-BN powder mixture (10:1 wt% ratio) inside a cylindrical sleeve of boron nitride. The NaCl powder was also used as an internal pressure standard and the cell pressure was calculated from its equation of state (Decker, 1971). The uncertainties in pressure are about 0.2 GPa in the P-T range of this study, mainly resulting from the uncertainties of the lattice parameters of NaCl measured under each experimental condition. The temperature was measured by a W/Re25%-W/Re3% thermocouple with the thermal junction placed adjacent to the specimen (e.g., Li et al. 2004). The vertical and radial temperature gradients over the entire sample chamber were estimated to be less than 20 K/mm (Weidner et al., 1992).

The sample was initially compressed to the highest pressure (7.7 GPa) at room temperature, followed by a resistivity heating to the peak temperature of 1173 K. Subsequently, the experiment was continued via a series of cooling/heating cycles at various pressures in the stability field of aragonite, during which data were collected at temperature of 1173, 973, 773, and 300 K. From 773 to 300 K, the temperature was quenched to room temperature by switching off the power supply to avoid the formation of calcite. Note that our data were collected along cooling to room temperature after reaching the peak temperature at each designated pressure to minimize the effect of deviatoric stress generated during compression/decompression at room-temperature (Wang et al., 1994). To avoid the occurrence of phase transition and disordered structure (Suito et al., 2001; Ono et al., 2005), X-ray diffraction of the sample under the entire P-T conditions was closely monitored, and the results confirmed that the specimen remained in pure aragonite and there was no phase transition throughout the course of the current experiment.

X-ray diffraction data were recorded in energy dispersive mode using a solid-state Ge detector. The lattice parameters and thus densities at high P-T were obtained by Le Bail full spectrum fit (Le Bail, 2005) using the software package GSAS (Larson and Von Dreele, 2000) and the EXPGUI (Toby, 2001). P and S wave travel times were obtained by pulse echo overlap (PEO) method. Details of the experimental setup for the ultrasonic interferometry in multi-anvil apparatus have been described elsewhere (Li et al., 2014). The precision of our P and S travel time measurements is about 0.2 ns. Sample lengths at high P-T were obtained from the X-ray images recorded by the CCD camera (e.g., Li et al, 2014), the uncertainty with respect to pixel number is 0.2~0.4%.

### 3 Results

The measured  $V_p$  and  $V_s$  velocities of the aragonite sample at high P-T are summarized in Figure (see also table S1). The velocities of both  $V_p$  and  $V_s$  increased

with increasing pressure at constant temperature and decreased with increasing temperature at constant pressure in the experimental P-T ranges. At room temperature, the  $V_p$  velocity increased from 6.43 km/s to 6.68 km/s when pressure increased from 0.9 GPa to 3.63 GPa, yielding an average pressure derivative of  $0.091 \text{ km/s} \cdot \text{GPa}^{-1}$ , and the  $V_s$  velocity increased from 3.51 km/s to 3.55 km/s within the same experimental pressure range, yielding a pressure derivative of  $0.014 \text{ km/s} \cdot \text{GPa}^{-1}$ . The average temperature derivatives of P and S waves are  $-5.81 \times 10^{-4} \text{ (km/s)} \cdot \text{K}^{-1}$ , and  $-3.18 \times 10^{-4} \text{ (km/s)} \cdot \text{K}^{-1}$ , respectively. The measurements of  $V_p$  and  $V_s$  velocities at room pressure and temperature were respectively 6.33 km/s and 3.49 km/s, which are comparable with the values determined by Brillouin spectroscopy under ambient conditions (Liu et al., 2005). The wave velocities of aragonite are lower than those of all major minerals in subducted slab and surrounding mantle, such as olivine, orthopyroxene, garnet and clinopyroxene.  $V_p/V_s$  ratio of the aragonite under room temperature and pressure is 1.81.

Adiabatic bulk ( $K$ ) and shear ( $G$ ) moduli under the high P-T conditions were calculated using  $V_p$  and  $V_s$  velocities and density by  $K = \rho(V_p^2 - 4V_s^2/3)$  and  $G = \rho V_s^2$ , and the results were tabulated in Table S1. To obtain the elastic moduli and their derivatives of pressure and temperature under ambient conditions, all the observed data of velocity and density were fitted to the third-order finite strain equations (Davies and Dziewonski, 1975), yielding  $K_0 = 69.39(5) \text{ GPa}$ ,  $K_0' = 4.8 (3)$ ,  $(\partial K/\partial T)_P = -0.020 (6) \text{ GPa/K}$ ,  $G_0 = 35.5 (4) \text{ GPa}$ ,  $G_0' = 1.1 (1)$ ,  $(\partial G/\partial T)_P = -0.009 (1) \text{ GPa/K}$ . The zero-pressure thermal expansion coefficient ( $\alpha_0 = 4.2 \times 10^{-5} + 6.4 \times 10^{-8} T$ ) of the aragonite was constrained based on the state equation and P-V-T analysis reported by Li et al. (2015) to minimize the standard error of fitting. The presenting direct constraints on  $(\partial K_s/\partial T)_P$ ,  $G'$ , and  $(\partial G/\partial T)_P$  that have never been reported before yielded a set of elasticity data that were more complete and self-consistent. The current values of bulk and shear moduli at ambient pressure are in good agreement with the results of a lattice dynamical calculation by Sekkal et al. (2008), and within mutual uncertainties of the single-crystal data from Brillouin scattering measurements (Liu et al., 2005). Our results also fall in the range of predicted values for  $K_{S0}$  and  $K_{S0}'$  and  $(\partial K_s/\partial T)_P$  by Santos et al (2020) based on LDA, GGA-PBE and vdW-DF approximations spanning from 61.9 ~ 75.7, 4.17 ~ 4.77, and -0.015 ~ -0.022, respectively (Table 1). Taking into consideration of the trade-off among  $K_T$ ,  $K_T'$ ,  $(\partial K/\partial T)_P$ , and thermal expansion coefficients, the values of isothermal bulk modulus  $K_T$  and its pressure derivative  $K_T'$  of aragonite were calculated to be  $K_T = 67.7(5) \text{ GPa}$ ,  $K_T' = 4.84 (3)$ ,  $(\partial K_T/\partial T)_P = -0.026(5) \text{ GPa/K}$ , which are consistent with the previous data of  $K_T$  and  $K_T'$  measured by X-ray diffraction ranged from 65.24 ~ 67.1(63) and 4.7(8) ~ 5.1(1), respectively (Ono et al., 2005; Li et al., 2015; Palaich et al., 2016; Litasove et al., 2017). when  $K_T$  and  $K_T'$

216 and thermal expansion coefficients (a and b) are constrained at the XRD values of Li et  
217 al. (2015), fitting to our data yields  $(\partial K/\partial T)_P = -0.026(5)$  (GPa/K) which is in excellent  
218 agreement with the value of  $-0.024(2)$  GPa/K.

219

Table 1. Comparison of the elastic moduli of aragonite from present study and previous works

Reference	Method	$K_0$	$K_0'$	$\partial K / \partial T$	$G_0$	$G_0'$	$\partial G / \partial T$	$\alpha_0(10^{-5})$	$\alpha_1(10^{-8})$	P-T range
1	DFT(GGA-PBE) <sup>a</sup>	61.9	4.34							
	DFT(LDA) <sup>a</sup>	79.1	4.77	-0.022						
	DFT(optB86 b-vdW) <sup>a</sup>	75.7	4.17	-0.015						
2	Lattice dynamical calculation <sup>c</sup>	69.4			30.3					80GPa
3	BS <sup>a</sup>	68.9(14)			35.8(2)					0
4	XRD <sup>b</sup>	67.1(63)	4.7(8)							80GPa
5	XRD <sup>b</sup>	66.5(7)	5.0(1)					4.9(2)	3.7(5)	36GPa
6	XRD(VR) <sup>b</sup>	65.7(8)	5.1(1)	-0.016(1)				4.98(22)	2.81(31)	29GPa, 1673K
	XRD(BM) <sup>b</sup>	67.0(8)	4.7(1)	-0.016(1)				4.95(22)	2.77(40)	
7	XRD <sup>b</sup>	64.8(43)	4	-0.018				6.5(5)	0.3(3)	7GPa, 1073K
8	XRD <sup>b</sup>	65.24	4.95	-0.024(2)				4.2(4)	6.4(10)	5.8GPa, 1173K
9	US <sup>a</sup>	69.39(5)	4.8(2)	-0.020 (6)	35.5(2)	1.1 (1)	-0.009(1)	4.2*	6.4*	5.8GPa, 1173K
	Calculated <sup>b</sup>	67.7(5)	4.8(3)	-0.026 (5)						

220

<sup>1</sup>Santos et al. (2020). <sup>2</sup>Sekkal et al. (2008).  $G_0$  is calculated using VRH method. <sup>3</sup>Liu et al. (2005). <sup>4</sup>Ono et al. (2005). <sup>5</sup>Palaich et al. (2016). <sup>6</sup>Litasove et al. (2017). VR is

221

Vinet- Rydberg EOS; BM is Birch- Murnaghan EOS. <sup>7</sup> Martinez et al. (1996). <sup>8</sup>Li et al. (2015). <sup>9</sup>This study. \*value were fixed during data fitting. <sup>a</sup>  $K_S$ , <sup>b</sup>  $K_T$ , <sup>c</sup> 0K (DFT)

222

calculation, DFT, density function theory; BS, Brillouin scattering spectroscopy; XRD, static compression X-ray diffraction; US, ultrasonic interferometry;  $K_T = K_S / (1 + \alpha \gamma T)$

223

(Poirier, 2000);  $\alpha = \alpha_0 + \alpha_1 T$ ;

224

$(\partial K_T / \partial T)_P \approx (\partial K_S / \partial T)_P / (1 + \alpha \gamma T) - K_S / (1 + \alpha \gamma T)^2 [\alpha \gamma + (\partial \alpha / \partial T)_P T]$  (Jiang et al., 2004);

225

$(\partial K_T / \partial P)_T = (1 + \alpha \gamma T)^{-1} [(\partial K_S / \partial P)_T - \gamma T / K_T (\partial K_T / \partial T)_P]$  (Poirier, 2000; Jiang et al., 2004)



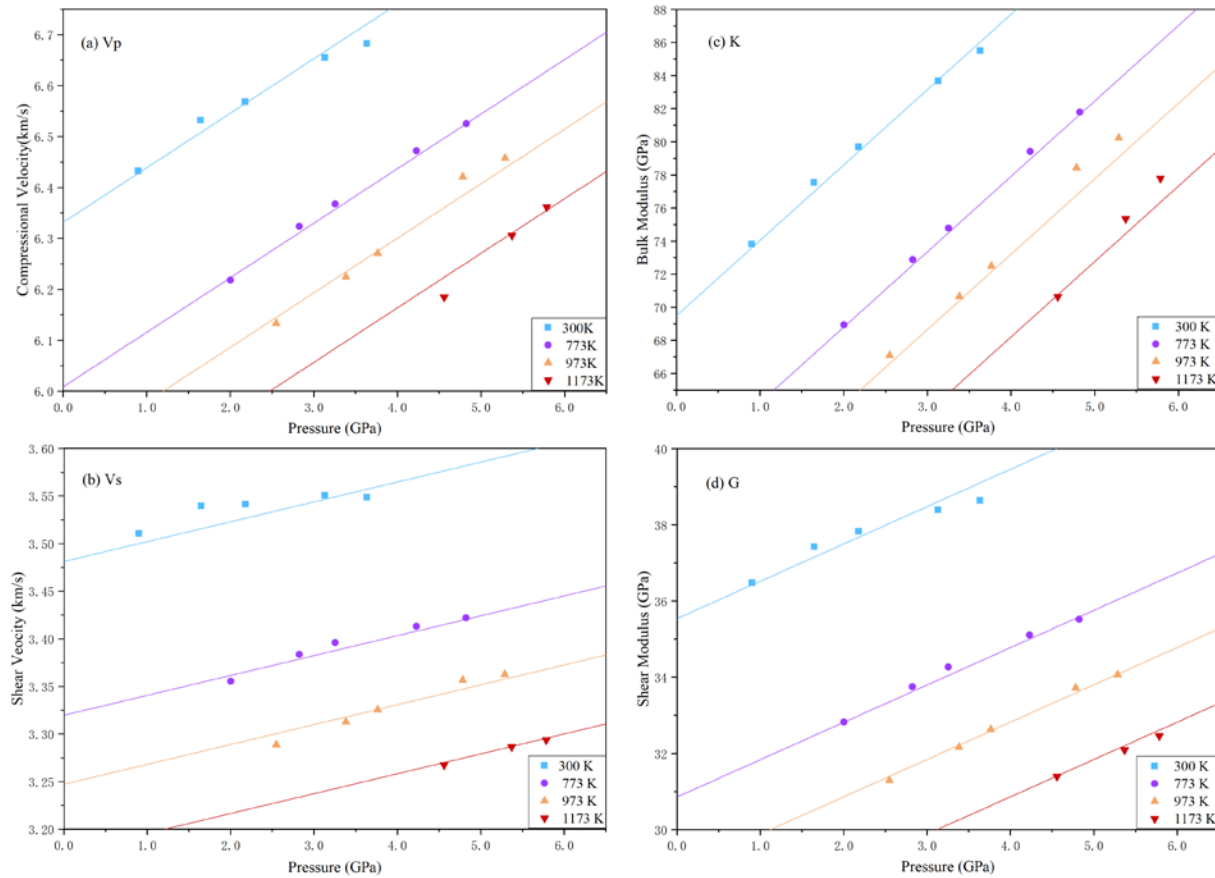


Figure 1. (a) Compressional ( $V_p$ ) and (b) shear ( $V_s$ ) wave velocities, (c) bulk ( $K$ ) and (d) shear ( $G$ ) moduli at high pressure and high temperature. The colored lines are calculated by finite strain method along experimental isotherms.

#### 4 Discussion and Implications

Altered basaltic oceanic crust may contain 2.5wt%  $\text{CO}_2$ , these carbonated-basalts, along with carbonatitic ocean sediments, subducted into deep earth and thus have impact both on the physical and chemical properties of subduction zone and upper mantle. Therefore, based on the elastic moduli of aragonite from this study as well as elasticity data for major mantle minerals and carbonates from previous studies (Table S2),  $V_p$ ,  $V_s$  and  $V_p/V_s$  of each mineral at relevant pressure and temperature were calculated and compared. The P-T path are along two typical geotherms for cold and hot subducted slabs of southwest and northeast Japan. In a realistic case, most the geotherm may lie in between the two (Peacock & Wang, 1999; Kerrick & Connolly, 2001). Results show that  $V_p$  and  $V_s$  of minerals along hot subduction zone slightly slower than those of cold subduction zone, and increase with pressure, except for aragonite and magnesite, the  $V_s$  of which were reduced under 2 GPa along hot subduction geotherm. Note that  $V_p$  and  $V_s$  of most minerals decrease with increasing pressure at 2 ~ 3 GPa due to the fast elevation of temperature at 60 ~ 80 km depth. Within 0 ~ 6 GPa,  $V_p$  and  $V_s$  velocities of the aragonite are 26 ~ 33% and 23 ~ 33%

244 slower than that of mantle minerals, respectively. We also calculated  $V_p/V_s$  of aragonite and  
245 compared with mantle minerals along hot and cold geotherms. As shown in Figure 2,  $V_p/V_s$  of  
246 aragonite increases monotonically from 1.82 to 1.92 in both hot and cold subduction zones, and  
247 shows nearly no sensitivity to temperature. In comparison,  $V_p/V_s$  of other minerals exhibits values  
248 ranging from 1.67 ~ 1.82, which are much smaller than that of aragonite. Furthermore,  $V_p/V_s$  of  
249 aragonite increases more rapidly with increasing pressure, while  $V_p/V_s$  of garnet shows the least  
250 variation with depth in both hot and cold subduction zones.

251 Combining the phase diagram of  $\text{CaCO}_3$  and geotherm data (Hess et al., 1991; Suito et al.,  
252 2001), calcite I transforms to aragonite at 1 GPa along hot subduction zone geotherm and at 1.3  
253 GPa along cold subduction zone geotherm. In this study, calcite II is neglected due to the narrow  
254 P-T range due to its narrow existing pressure range (~ 0.2 GPa). The velocities of calcite are plotted  
255 in Figure 2. It is obvious that calcite and aragonite have similar  $V_s$ , but calcite has a greater (~ 6%)  
256  $V_p$  than aragonite. Furthermore, calcite has a  $V_p/V_s$  of ~ 7% higher than aragonite. These  
257 observations suggest that the transformation of calcite to aragonite at depth 30 ~ 40 km may cause  
258 sharp decrease of  $V_p$  and  $V_p/V_s$ . By comparison, velocities and  $V_p/V_s$  of magnesite are close to  
259 those of olivine, orthopyroxene and clinopyroxene along cold and hot subduction geotherms,  
260 indicating that a composition change from aragonite-rich to magnesite-rich carbonate assemblages  
261 would decrease the seismic detectability of velocity perturbations caused by carbonates in  
262 subducting process.

263

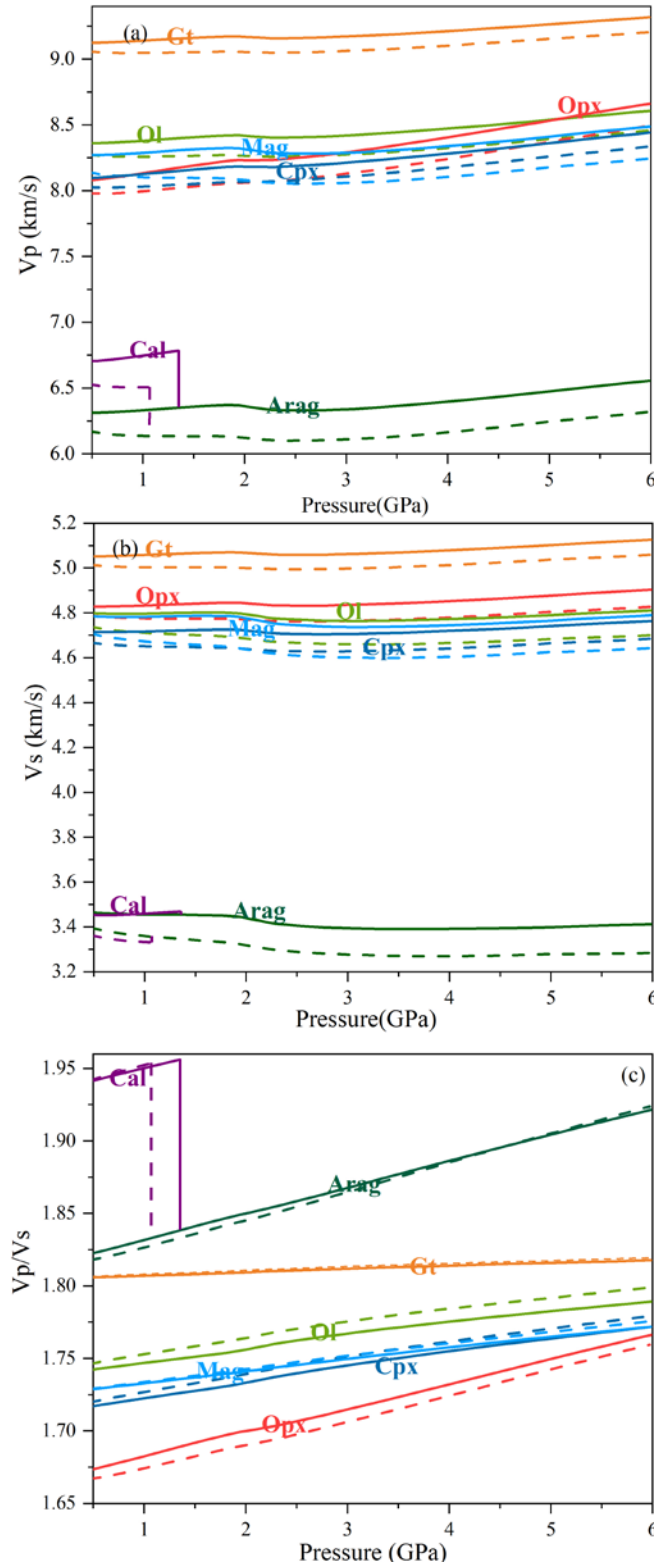


Figure 2. P (a) and S wave (b) velocities and  $V_p/V_s$  (c) of minerals at relevant pressure and temperature conditions of the subduction zone. Solid and dashed lines are the velocities along the subduction zone in Northeast (cold) and Southwest (hot) Japan, respectively.

According to the possible content of aragonite in subduction zone, the velocities of carbonated eclogite and carbonated peridotite that contain 2.5 wt.% CO<sub>2</sub> along hot and cold subduction zone are modeled and calculated (Alt and Teagle, 1999). The composition of unaltered ocean crust in forms of eclogite that composed of approximately 53.5wt.% garnet and 46.7wt.% clinopyroxene, while upper mantle is mainly composed of peridotite, which consists of 59.3wt.% olivine, 12.8wt.% clinopyroxene, 11.4wt.% orthopyroxene, and 16.5wt.% garnet (Dasgupta et al., 2004; Dasgupta and Hirschmann, 2005; Yang et al., 2014). The mineral proportions that contain 2.5 wt.% CO<sub>2</sub> were recalculated by a normalization with respect to the new total. Based on the density, elastic moduli, and volume proportions of minerals, sound velocities for carbonated-eclogite and carbonated-peridotite are calculated following the procedures described in Cottaar et al., (2014).

Both carbonated eclogite and carbonated peridotite that contains 2.5wt% CO<sub>2</sub> in forms of aragonite and magnesite were modeled and compared, as magnesite is more stable in the deeper mantle, and Ca would gradually instead by Mg during subduction process, to form dolomite (CaMg(CO<sub>3</sub>)<sub>2</sub>, magnesite (MgCO<sub>3</sub>), as well as siderite (FeCO<sub>3</sub>) according to the field observations and experiments. The mechanism of Mg enrich may be (1) Ion exchange between aragonite and magnesium silicate in subducted slabs or with surrounding mantle through the reaction of  $6\text{CaCO}_3(\text{calcite}) + \text{Mg}_3\text{Al}_2\text{Si}_3\text{O}_{12}(\text{pyrope}) = 3\text{CaMg}(\text{CO}_3)_2(\text{dolomite}) + \text{Ca}_3\text{Al}_2\text{Si}_3\text{O}_{12}(\text{grossular})$  and  $\text{Mg}_2\text{Si}_2\text{O}_6(\text{orthoenstatite}) + 2\text{CaCO}_3(\text{calcite}) = \text{CaMgSi}_2\text{O}_6(\text{diopside}) + \text{CaMg}(\text{CO}_3)_2(\text{dolomite})$  will lead to the stability shifts along the solidus of carbonated lithologies from calcite (aragonite) to dolomite to magnesite-rich component. Velocity effect caused by ion exchange of carbonated eclogite was also evaluated using previous experiment data (Dasgupta et al. 2005). Basalt with 2.2wt% CO<sub>2</sub>(5% calcite) was used as sample in the experiment, which CO<sub>2</sub> content is comparable to our model, was conducted under excess heating conditions relative to hot subduction zone (3GPa, 1100°C). After the experiment, ~25% of calcite (1.25wt% in total) transform to MgCO<sub>3</sub> and FeCO<sub>3</sub>, these velocity effect caused by transition of grossular to pyrope or diopside to enstatite are all negligible due to the low ion exchange ratio and similar elastic constant (Table S2); (2) Ca is dissolved more efficiently than Mg, the dehydration of the oceanic crust will extract calcium rich fluid, thus the Mg/Ca ratio is elevated with the dehydration of hydrous minerals (Dasgupta et al., 2004). Without considering the existence of fluid in system, the two mechanism of decalcification are all available in our model.

The elastic moduli of dolomite is assumed to be identical to that of a mechanical mixture of Ca and Mg endmembers, and can be obtained from VRH approximation. The calculated velocities of dolomite are between that of aragonite and magnesite. Siderite (FeCO<sub>3</sub>) may also be generated during subduction process (Molina & Poli, 2000), the velocities of siderite are lower than those of magnesite but comparable to aragonite at room temperature, at high pressure and temperature, velocities of FeCO<sub>3</sub> bearing magnesite is slower than that of magnesite, although its velocities under high temperature conditions compared with aragonite still needs further investigations (Sanchez-Valle et al., 2011; Merlini et al., 2016; Chariton et al., 2020). Thus the magnesite that has high elastic parameters relative to other carbonates (dolomite, siderite etc.) may

constrain the upper limits of velocities in carbonated subduction slabs. As shown in Fig. 3, P and S wave velocities along cold subduction slab are ~1% higher than those along hot subduction zone. The presence of 5.68% aragonite (2.5wt.% CO<sub>2</sub>) in eclogite and peridotite results in 2.1 ~ 2.4% for V<sub>P</sub> and 2.4 ~ 2.9% for V<sub>S</sub> velocity perturbations relative to pure eclogite and peridotite. However, as shown above, the velocity contrast between magnesite-eclogite (magnesite-peridotite) and pure eclogite (peridotite) becomes negligible (see Fig. 3(a, b)). We also calculated the V<sub>P</sub>/V<sub>S</sub> ratio of eclogite and peridotite assemblages. As shown in Fig. 3 (c, d), aragonite bearing assemblages have the highest V<sub>P</sub>/V<sub>S</sub> ratio, ranging from ~1.74 to 1.81 within 0.4 ~ 6 GPa.

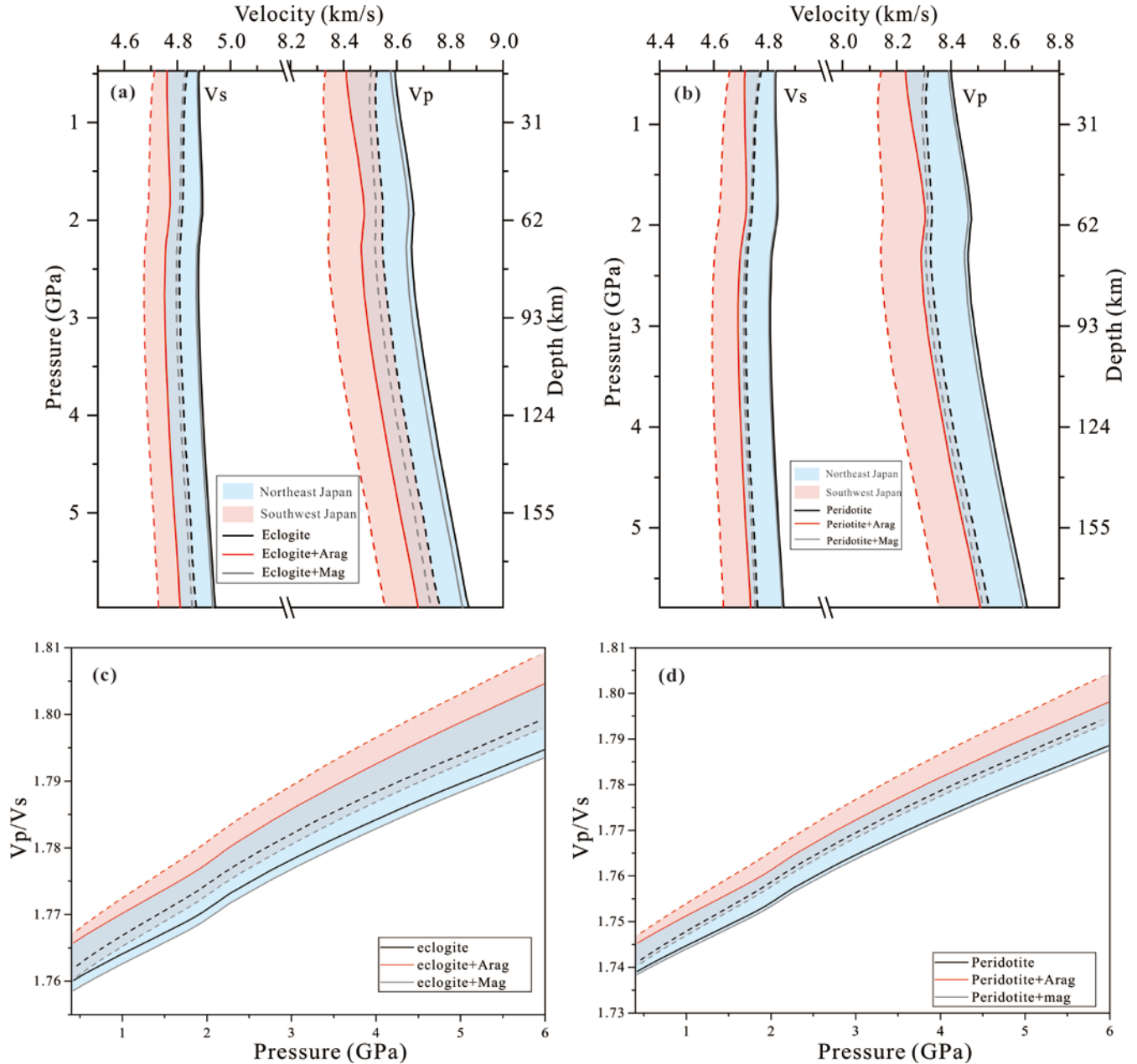


Figure 3. The V<sub>P</sub> and V<sub>S</sub> and V<sub>P</sub>/V<sub>S</sub> of (a), (c) carbonated eclogite compared with eclogite (b), (d) carbonated peridotite compared with peridotite at relevant pressure and temperature conditions of

the subduction zone. Solid and dashed lines are the velocities along the subduction zone in Southwest (hot) and Northeast (cold) Japan, respectively.

Presence of aragonite may enhance the observation of low seismic-velocity layer (LVL). In many subduction zones around Pacific Ocean, seismic observations reveal the presence of low seismic-velocity layer coinciding with the zone of thrust and intermediate-depth earthquakes (Peacock & Wang, 1999; Abers, 2005; Nakajima et al., 2006). The velocity anomalies of most LVL are reported to be 3 ~ 14% slower than its surroundings at shallow mantle but diminishing at depth within 150 ~ 250 km (Abers, 2000; Abers, 2005; Nakajima et al., 2006). Lawsonite has been proposed to be the candidate causing LVL at depth  $> 90$  km due to its stability at higher pressure and the low elastic moduli, followed by the diminishing of minerals with high elastic moduli during subduction processes, such as garnet and olivine (Kerrick & Connolly, 2001; Chantel et al., 2012). Thus, we compared the velocities of aragonite with hydrous minerals including lawsonite, antigorite, aragonite, and phase A (Figure S2). We found the velocities of aragonite is second only to antigorite, but much lower than that of lawsonite, although lawsonite has much higher  $V_P/V_S$  ratio. Furthermore, fully hydrate eclogite that contains as large as 20 vol% lawsonite is required to reproduce a seismic velocity anomaly of 2% for  $V_P$  and 5% for  $V_S$  in maximum. It may not enough to explain higher anomalies around Pacific subduction zone, such as ~ 3%  $V_P$  anomaly observed at 220 km depth in the subduction zone forearc of northern Japan (Garth & Rietbrock, 2014). Based on our calculations, it requires 7.1 ~ 8.3 wt.% aragonite (3.1 ~ 3.7 wt.%  $\text{CO}_2$ ) in eclogite to reproduce the 3% anomaly in  $V_P$  observed in the subduction zone forearc of northwestern Japan, together with 3.5% reduction in  $V_S$ . Considering that there is only 2.5 wt.%  $\text{CO}_2$  in subducted oceanic crust, ~ 5 vol% lawsonite is still required to jointly produce the seismically observed variations of 3% in  $V_P$  and 4.3% in  $V_S$  at LVL. Low velocity and high  $V_P/V_S$  layer are also observed in northeast Japan and coincides with electrically conductive zones (Nakajima et al., 2006; Tsuji et al., 2008). The origin of electrical conductivity is generally considered as fluid, melt or cracks (Wang et al., 2012). Our data suggest that the LVL is caused jointly by the existence of lawsonite and aragonite, and the presence of aragonite can be an alternative candidate to lead to the observation of LVL and electrically conductive zones.

In the discussion above, whether ion exchange reaction or dehydration may cause Mg enrich in carbonates, these reaction may coincide with the dehydration of lawsonite, and cause the decay of low velocity anomalies in depth  $> 250$  km. Alternative chemical interaction pathways, such as suggested by the reaction of  $\text{CaCO}_3 + \text{SiO}_2 = \text{CaSiO}_3 + \text{CO}_2$  (Litasov et al., 2017) under ultra-high temperature or  $\text{CaCO}_3 + \text{SiO}_2 = \text{CaSiO}_3 + \text{C} + \text{O}_2$  in redox environment may also occur, which may also have significant influence on velocities of subduction zone (Frezzotti et al., 2011; Galvez et al., 2013). However, experiment shows that carbonate melts generated from carbonated eclogite may be at depths up to 410 km, which depth is consistent with the low velocity layer atop of transition zone and lead to sharp decrease of  $V_P$  and  $V_S$  in subduction zone and observed in most of subduction zones such as the western U.S. (Thomson et al., 2016; Han et al., 2020); Furthermore, solidus of carbonated upper mantle is lower than the upper mantle adiabat, carbonated silicate melt

generated at deep of 220 ~ 300 which may explain the phenomenon of seismic observing X discontinuity (Dasgupta et al., 2013). These observations suggests carbonates would stable at mantle depth, and thus has impact influence on the velocities in subduction zone.

Over all, aragonite is an important mineral phase that has low  $V_p$ ,  $V_s$  and high  $V_p/V_s$  among subduction zone minerals. At shallow depths, transformation of calcite I to aragonite occurring at depth of 30 ~ 40 km in the subduction zone is expected to cause sharp decrease of  $V_p$  and  $V_p/V_s$ . The aragonite subducted into deep earth may be manifested by distinctive physical property changes in a wide depth range, causing detectable low velocity anomalies of seismic wave. With 2.5 wt.%  $\text{CO}_2$  in forms of aragonite in subducted ocean crust, velocity perturbations up to 2.1 ~ 2.4% for  $V_p$  and 2.4 ~ 2.9% for  $V_s$  can be produced. The elastic properties attained by this study shed lights on the seismic characteristics associates with these chemical reactions and phase changes.

## Acknowledgments

This work is supported financially by the National Science Foundation of China (Grant No. 42073063), National Key Research and Development Program of China (Grant No. 2019YFC1509203), Key Laboratory of Earthquake prediction, Institute of Earthquake Forecasting, CEA (Grant No. 2017KLEP03).

## Conflict of Interest

The authors declare no conflicts of interest relevant to this study.

## Data Availability Statement

Experimental data for Figure 1 are listed in table S1. More detailed information of experimental results and data is available in supporting information. The experimental data archiving is underway. We are going to upload the data to <https://www.earthchem.org/>.

## References

Abers, G. A., 2005. Seismic low-velocity layer at the top of subducting slabs: Observations, predictions, and systematics. *Physics of the Earth and Planetary Interiors*, 149, 7–29.

<https://doi.org/10.1016/j.pepi.2004.10.002>

- Alt, J. C., Schwarzenbach, E. M., Früh-Green, Gretchen L., Shanks, W. C., Bernasconi, S. M., & Garrido, C. J., et al., 2013. The role of serpentinites in cycling of carbon and sulfur: seafloor serpentinitization and subduction metamorphism. *Lithos*, 178, 40-54.  
<https://doi.org/10.1016/j.Lithos.2012.12.006>
- Berner, R. A., Honjo, S., 1981. Pelagic sedimentation of aragonite: its geochemical significance. *Science*, 211, 940-942. <https://doi:10.1126/science.211.4485.940>
- Chantel, J., Mookherjee, M., Frost, D. J., 2012. Low velocity layer (LVL) in subduction zones: elasticity of lawsonite. *Earth and Planetary Science Letters*, s349–350(4):116-125.  
<https://doi.org/10.1016/j.epsl.2012.06.034>
- Chariton, S., Mccammon, C., Vasiukov, D. M., et al., 2020. Seismic detectability of carbonates in the deep earth: a nuclear inelastic scattering study. *American Mineralogist* , 105(3), 325-332. <https://doi.org/10.2138/am-2020-6901>
- Chen, P.F., Chiao, L.Y., Huang, P.H., et al., 2006. Elasticity of magnesite and dolomite from a genetic algorithm for inverting Brillouin spectroscopy measurements. *Physics of the Earth and Planetary Interiors*, 155(1-2), 73-86. <https://doi.org/10.1016/j.pepi.2005.10.004>
- Cottaar, S., Heister, T., Rose, I., Unterborn, C., 2014. BurnMan: a lower mantle mineral physics toolkit. *Geochemistry, Geophysics, Geosystems*, 15, 1164–1179.  
<https://doi.org/10.1002/2013GC005122>
- Dasgupta, R., Mallik, A., Tsuno, K., Withers, A. C., Hirth, G., Hirschmann, M. M., 2013. Carbon-Dioxide-Rich Silicate Melt in the Earth’s Upper Mantle. *Nature*, 493(7431), 211–15. <https://doi.org/10.1038/nature11731>
- Dasgupta, R., Hirschmann, M. M., Withers, A.C., 2004. Deep global cycling of carbon constrained by the solidus of anhydrous, carbonated eclogite under upper mantle conditions.



*Earth and Planetary Science Letters*, 227(1–2): 73–85.

<https://doi.org/10.1016/j.epsl.2004.08.004>

Dasgupta, R., Hirschmann, M. M., & Dellas, N., 2005. The effect of bulk composition on the solidus of carbonated eclogite from partial melting experiments at 3GPa. *Contributions to Mineralogy and Petrology*, 149(3), 288–305. <https://doi.org/10.1007/s00410-004-0649-0>

Davies, G. F., Dziewonski, A. M., 1975. Homogeneity and constitution of the earth's lower mantle and outer core. *Physics of the Earth and Planetary Interiors*, 10(4), 336–343.

[https://doi.org/10.1016/0031-9201\(75\)90060-6](https://doi.org/10.1016/0031-9201(75)90060-6)

Decker, D.L., 1971., High-pressure equation of state for NaCl, KCl, and CsCl. *Journal of Applied Physics*, 42, 3239–3244. <https://doi.org/10.1063/1.1660714>

Fisler, D.K., Gale, J.D., Cygan, R.T., 2000. A shell model for the simulation of rhombohedral carbonate minerals and their point defects. *American Mineralogist*, 85, 217–224.

<https://doi.org/10.2138/am-2000-0121>

Frezzotti, M.L., Selverstone, J., Sharp, Z. D., Compagnoni, R., 2011, Carbonate dissolution during subduction revealed by diamond-bearing rocks from the Alps. *Nature*, 4, 703–706.

<https://doi.org/10.1038/ngeo1246>

Galvez, M. E., Beyssac, O., Martinez, I., et al., 2013. Graphite formation by carbonate reduction during subduction. *Nature Geoscience*, 6, 473–477. <https://doi.org/10.1038/ngeo1827>

Garth, T., Rietbrock, A. Dondip velocity changes in subducted oceanic crust beneath Northern Japan—insights from guided waves. *Geophysical Journal International*, 2014, 198(3), 1342–1358. <https://doi.org/10.1093/gji/ggu206>

Hacker, B.R., 1996. Eclogite formation and the rheology, buoyancy, seismicity, and H<sub>2</sub>O content of oceanic crust. *American Geophysical Union*, pp. 337-346.

<https://doi.org/10.1029/GM096p0337>

Han, G., Li, J., Guo, G., Mooney, W. D., Karato, S., Yuen, A. D., 2020. Pervasive Low-Velocity Layer atop the 410-Km Discontinuity beneath the Northwest Pacific Subduction Zone: Implications for Rheology and Geodynamics. *Earth and Planetary Science Letters*, 554:

116642. <https://doi.org/10.1016/j.epsl.2020.116642>

Hess, N. J., Ghose, S., Exarhos, G. J., 1991. Raman spectroscopy at simultaneous pressure and temperature: Phase relations and lattice dynamics of CaCO<sub>3</sub>. Proceedings XIII th AIRAPT international conference on high pressure science and technology, Oxford, New Delhi. 236–241.

Jiang, F., Speziale, S., Duffy, T. S. 2004. Single-crystal elasticity of grossular- and almandine-rich garnets to 11 gpa by brillouin scattering. *Journal of Geophysical Research*, 109(10), 1-10. <https://doi.org/10.1029/2004JB003081>

Kelemen, P. B., Manning, C. E., 2015. Reevaluating carbon fluxes in subduction zones, what goes down, mostly comes up. *Proceedings of the National Academy of Sciences of the United States of America*, 112(30), 3997-4006. <https://doi.org/10.1073/pnas.1507889112>

Kerrick, D. M., Connolly, J. A. D., 2001. Metamorphic devolatilization of subducted marine sediments and the transport of volatiles into the Earth's mantle. *Nature*, 411, 293-6.

<https://doi.org/10.1038/35077056>

Kondo, S., Suito, K. & Matsushima, S., 1972. Ultrasonic observation of calcite I-II inversion to 700°C. *J. Journal of Physics of the Earth*, 20, 245–250.

<https://doi.org/10.4294/jpe1952.20.245>

- 456 Larson, A.C., and Von Dreele, R.B., 2000. General Structure Analysis System (GSAS). Los  
457 Alamos National Laboratory Report LAUR, 86-748.
- 458 Li, B., Kung, J., Liu, W., Liebermann, R. C., 2014. Phase transition and elasticity of enstatite  
459 under pressure from experiments and first-principles studies. *Physics of the Earth and*  
460 *Planetary Interiors*, 228, 63–74. <https://doi.org/10.1016/j.pepi.2013.11.009>
- 461 Li, Y., J. Du, X. Wang, X. Zhou, C. Xie, and Y. Cui, 2013. Spatial variations of soil gas  
462 geochemistry in the Tangshan area of Northern China. *Terrestrial, Atmospheric and*  
463 *Oceanic Sciences journal*, 24, 323-332. [https://doi.org/10.3319/TAO.2012.11.26.01\(TT\)](https://doi.org/10.3319/TAO.2012.11.26.01(TT))
- 464 Li, Y., Zou, Y. T, Chen, T., Wang, X.B., Qi, X.T., Chen, H.Y., Du, J.G., Li, B.S., 2015. P-V-T  
465 equation of state and high-pressure behavior of CaCO<sub>3</sub> aragonite, *American Mineralogist*,  
466 100, 2323-2329. <https://doi.org/10.1016/j.pepi.2017.02.006>
- 467 Liu, L. G, Chen, C. C., Lin, C. C., 2005. Elasticity of single-crystal aragonite by Brillouin  
468 spectroscopy. *Physics and Chemistry of Minerals*, 32(2), 97-102.  
469 <https://doi.org/10.1007/s00269-005-0454-y>
- 470 Lobanov, S. S., Dong, X., Martirosyan, N. S., Samtsevich, A. I., Stevanovic, V., Gavryushkin, P.  
471 N., Litasov, K. D., Greenberg, E., Prakapenka, V. B., 2017. Raman spectroscopy and x-ray  
472 diffraction of sp<sup>3</sup> CaCO<sub>3</sub> at lower mantle pressures, *Physical Review B*, 96(10), 104101.  
473 <https://doi.org/10.1103/PhysRevB.96.104101>
- 474 Martinez, I., Zhang, J.Z., Reeder, R.J., 1996. In situ X-ray diffraction of aragonite and dolomite  
475 at high pressure and high temperature: Evidence for dolomite breakdown to aragonite and  
476 magnesite. *American Mineralogist*, 81, 611-624. <https://doi.org/10.2138/am-1996-5-608>

- Molina, J. F. & Poli, S., 2000. Carbonate stability and fluid composition in subducted oceanic crust: An experimental study on H<sub>2</sub>O–CO<sub>2</sub>–bearing basalts. *Earth and Planetary Science Letters*, 176, 295310. [https://doi.org/10.1016/S0012-821X\(00\)00021-2](https://doi.org/10.1016/S0012-821X(00)00021-2)
- Nakajima, J., & Hasegawa, A., 2006. Anomalous low-velocity zone and linear alignment of seismicity along it in the subducted Pacific slab beneath Kanto, Japan: Reactivation of subducted fracture zone? *Geophysical Research Letters*, 33(16), 1–4. <https://doi.org/10.1029/2006GL026773>
- Ono, S., Kikegawa, T., Ohishi, Y., and Tsuchiya, J., 2005. Post-aragonite phase transformation in CaCO<sub>3</sub> at 40 GPa. *American Mineralogist*, 90, 667-671. <https://doi.org/10.2138/am.2005.1610>
- Palaich, S. E. M., Heffern, R. A., Hanfland, M., et al. 2016. High-pressure compressibility and thermal expansion of aragonite. *American Mineralogist*, 101(7), 1651-1658. <https://doi.org/10.2138/am-2016-5528>
- Peacock, S. M. & Wang, K., 1999. Seismic consequences of warm versus cool subduction metamorphism: Examples from Southwest and Northeast Japan. *Science*, 286, 937±939. <https://doi.org/10.1126/science.286.5441.937>
- Perchuk, A.L., and Korepanova, O.S., 2011. The problem of CO<sub>2</sub> recycling in subduction zones. *Moscow University Geology Bulletin*, 66, 250-260. <https://doi.org/10.3103/S0145875211040107>
- Poirier, J. P., 2000. Introduction to the Physics of the Earth's Interior. Cambridge University Press.

- Sanchez-Valle, C., Ghosh, S., Rosa, A. D., 2011. Sound velocities of ferromagnesian carbonates and the seismic detection of carbonates in eclogites and the mantle. *Geophysical Research Letters*, 38(24), 422-433. <https://doi.org/10.1029/2011GL049981>
- Santos, S. S. M., Marcondes, M. L., Justo, J. F., et al., 2020. Calcium carbonate at high pressures and high temperatures: A first-principles investigation. *Physics of the Earth and Planetary Interiors*, 299:106327. <https://doi.org/10.1016/j.pepi.2019.106327>
- Sekkal, W., Taleb, N., Zaoui, A. & Shahrour, I., 2008. A lattice dynamical study of the aragonite and post-aragonite phases of calcium carbonate rock. *American Mineralogist*, 93, 1608–1612. <https://doi.org/10.2138/am.2008.2820>
- Shilobreeva, S., Martinez, I., Busigny, V., Agrinier, P., Laverne, C., 2011. Insights into C and H storage in the altered oceanic crust: Results from ODP/IODP Hole 1256D. *Geochimica et Cosmochimica Acta*, 75, 2237–2255. <https://doi.org/10.1016/j.gca.2010.11.027>
- Suito, K., Namba, J., Horikawa, T., Taniguchi, Y., Sakurai, N., & Kobayashi, M., et al., 2001. Phase relations of  $\text{CaCO}_3$  at high pressure and high temperature. *American Mineralogist*, 86(9), 997-1002. <https://doi.org/10.2138/am-2001-8-906>
- Syracuse, E. M., van Keken, P. E. & Abers, G. A. The global range of subduction zone thermal models. *Physics of the Earth and Planetary Interiors*, 183, 73–90 (2010). <https://doi.org/10.1016/j.pepi.2010.02.004>
- Thomson, A.R., Walter, M.J., Kohn, S.C., Brooker, R.A., 2016. Slab melting as a barrier to deep carbon subduction. *Nature*, 529, 76-79. <https://doi.org/10.1038/nature16174>
- Toby, B.H., 2001. EXPGUI, a graphical user interface for GSAS. *Journal of Applied Crystallography*, 34, 210–213. <https://doi.org/10.1107/S0021889801002242>

- Tsuji, Y., Nakajima, J., Hasegawa, A., 2008. Tomographic evidence for hydrated oceanic crust of the pacific slab beneath northeastern japan: implications for water transportation in subduction zones. *Geophysical Research Letters*, 35(14), 236-238.  
<https://doi.org/10.1029/2008GL034461>
- Wang, X., Schubnel, A., Fortin, J., et al., 2012. High VP/VS ratio: Saturated cracks or anisotropy effects? *Geophysical Research Letters*, 39(11), 11307.  
<https://doi.org/10.1029/2012GL051742>
- Wang, Y., Weidner, D. J. Thermoelasticity of CaSiO<sub>3</sub> perovskite and implications for the lower mantle. *Geophysical Research Letters*, 1994, 21(10),895-898.  
<https://doi.org/10.1029/94GL00976>
- Yang, J., Mao, Z., Lin, J.-F., Prakapenka, V. B., 2014. Single-crystal elasticity of the deep-mantle magnesite at high pressure and temperature. *Earth and Planetary Science Letters*, 392, 292-299. <https://doi.org/10.1016/j.epsl.2014.01.027>
- Zhao, C. S., Li, H. P., Chen, P. F., Jiang, J. J., 2019. Sound velocities across calcite phase transitions by brillouin scattering spectroscopy. *American Mineralogist*, 104(3), 418-424.  
<https://doi.org/10.2138/am-2019-6682>
- Reference from the Supporting Information:
- Anderson, O. L., [Schreiber](#), E., & Liebermann, R. C., 1968. Some elastic constant data on minerals relevant to geophysics. *Reviews of Geophysics*, 6, 491-524.  
<https://doi.org/10.1029/RG006i004p00491>
- Arimoto, T., Gréaux, S., Irifune, T., Zhou, C., Higo, Y. 2015. Sound Velocities of Fe<sub>3</sub>Al<sub>2</sub>Si<sub>3</sub>O<sub>12</sub> Almandine up to 19 GPa and 1700 K. *Physics of the Earth & Planetary Interiors*, 246: 1–8.  
<https://doi.org/10.1016/j.pepi.2015.06.004>

- Fei, Y., 1995. Thermal expansion, in Mineral Physics and Crystallography: A Handbook of Physical Constants, AGU Ref. Shelf Ser., vol. 2, edited by T. J. Ahrens, pp. 283– 291, AGU, Washington, D. C. <https://doi.10.1029/RF002p0029>
- Gwanmesia, G. D., Wang, L., Heady, A., Liebermann, R. C, 2014. Elasticity and sound velocities of polycrystalline grossular garnet ( $\text{Ca}_3\text{Al}_2\text{Si}_3\text{O}_{12}$ ) at simultaneous high pressures and high temperatures. *Physics of the Earth & Planetary Interiors*, 228, 80-87. <https://doi.10.1016/j.pepi.2013.09.010>
- Gwanmesia, G. D., Zhang, J., Darling K., et al., 2006. Elasticity of polycrystalline pyrope ( $\text{Mg}_3\text{Al}_2\text{Si}_3\text{O}_{12}$ ) to 9 GPa and 1000 °C. *Physics of the Earth & Planetary Interiors*, 155(s3– 4), 179-190. <https://doi.10.1016/j.pepi.2005.10.008>
- Hartwig, J. & Galkin, V, 2021. Heat capacity, thermal expansion, and elastic parameters of pyrope. *Journal of Thermal Analysis and Calorimetry*, 144, 71-79. <https://doi.10.1007/s10973-020-09396-2>
- Jackson, J. M., Palko, J. W., Andraut D, et al., 2003. Thermal expansion of natural orthoenstatite to 1473 K. *European Journal of Mineralogy*, 15(3), 469-473(5). <https://doi.10.1127/0935-1221/2003/0015-0469>
- Kung, J., Jackson, I., Liebermann, R. C., 2011. High-temperature elasticity of polycrystalline orthoenstatite ( $\text{MgSiO}_3$ ). *American Mineralogist*, 96(4), 577-585. <https://doi.10.2138/am.2011.3632>
- Kung, J., Li, B., Uchida, T., Wang, Y., Neuville, D., Liebermann, R.C, 2004. In situ measurements of sound velocities and densities across the orthopyroxene parr; high-pressure clinopyroxene transition in  $\text{MgSiO}_3$  at high pressure. *Physics of the Earth and Planetary Interiors*, 147, 27–44. <https://doi.10.1016/j.pepi.2004.05.008>

- Li, B., Neuville, D. R., 2010. Elasticity of Diopside to 8GPa and 1073K and Implications for the Upper Mantle. Li, Baosheng, and Daniel R. Neuville. 2010. “Elasticity of Diopside to 8GPa and 1073K and Implications for the Upper Mantle.” *Physics of the Earth and Planetary Interiors*, 183(3–4), 398–403. <https://doi.10.1016/j.pepi.2010.08.009>
- Lin, C. C., 2013. Elasticity of Calcite: Thermal Evolution. *Physics and Chemistry of Minerals*, 40(2): 157–66. <https://doi.10.1007/s00269-012-0555-3>
- Litasov, K. D., Fei, Y., Ohtani, E., Kuribayash, T., Funakoshi, K., 2008. Thermal equation of state of magnesite to 32GPa and 2073K. *Physics of the Earth & Planetary Interiors*, 168(s 3–4), 191–203. <https://doi.10.1016/j.pepi.2008.06.018>
- Liu, W., Kung, J. & Li, B, 2005. Elasticity of San Carlos olivine to 8 GPa and 1073 K. *Geophysical Research Letters*, 32, 1–4. <https://doi.10.1029/2005GL023453>
- Liu, W., Li, B.S., 2006. Thermal equation of state of (Mg<sub>0.9</sub>Fe<sub>0.1</sub>)<sub>2</sub>SiO<sub>4</sub> olivine. *Physics of the Earth & Planetary Interiors*, 157, 188–195. <https://doi.10.1016/j.pepi.2006.04.003>
- Lucas, A., Mouallem-Bahout, M., Carel, C., Gaudé, J. & Matecki, M., 1999. Thermal expansion of synthetic aragonite condensed review of elastic properties. *Journal of Solid State Chemistry* 146, 73–78. <https://doi.10.1006/jssc.1999.8310>
- Mookherjee, M., Mainprice, D, 2014. Unusually large shear wave anisotropy for chlorite in subduction zone settings. *Geophysical Research Letters*, 41, 1506–1513. <http://doi.10.1002/2014GL059334>
- Qian, W., Wang, W., Zou, F., Wu, Z., 2017. Elasticity of orthoenstatite at high pressure and temperature: Implications for the origin of low V<sub>P</sub>/V<sub>S</sub> zones in the mantle wedge. *Geophysical Research Letters*, 45, 665–673 <http://doi.10.1002/2017GL075647>



- Stixrude, L., Lithgow-Bertelloni, C., 2005. Thermodynamics of Mantle Minerals—I. Physical Properties. *Geophysical Journal International*, 162(2): 610–632. <http://doi.10.1111/j.1365-246X.2005.02642.x>
- Ungureanu, G. C., Cossio, R., Prencipe, M., 2012. An *Ab-initio* assessment of thermo-elastic properties of CaCO<sub>3</sub> polymorphs: Calcite case. *Calphad*, 2012, 37(1), 25-33. <https://doi.org/10.1016/j.calphad.2011.12.007>
- Sanchez-Valle, C., Sinogeikin, S. V., Smyth, J. R., Bass, J. D., 2008. Sound Velocities and Elasticity of DHMS Phase A to High Pressure and Implications for Seismic Velocities and Anisotropy in Subducted Slabs. *Physics of the Earth and Planetary Interiors* 170(3–4):229–39. <https://doi.10.1016/j.pepi.2008.07.015>
- Wang, Y., Weidner D. J., Zhang, J., Gwanrnesia G. D., Liebermann, R. C., 1998. Thermal Equation of State of Garnets along the Pyrope-Majorite Join. *Physics of the Earth and Planetary Interiors*, 105(1–2): 59–71. [https://doi.org/10.1016/S0031-9201\(97\)00072-1](https://doi.org/10.1016/S0031-9201(97)00072-1)
- Yang, J., Mao, Z., Lin, J.-F., Prakapenka, V. B., 2014. Single-crystal elasticity of the deep-mantle magnesite at high pressure and temperature. *Earth and Planetary Science Letters*, 392, 292-299. <https://doi.org/10.1016/j.epsl.2014.01.027>
- Zhao, C. S., Li, H. P., Chen, P. F., Jiang, J. J., 2019. Sound velocities across calcite phase transitions by brillouin scattering spectroscopy. *American Mineralogist*, 104(3), 418-424. <https://doi.org/10.2138/am-2019-6682>